NMR Microscopy and Spectroscopy; Perfused Brain Slices and Microcoils

NHMFL

Blackband, S.J., UF Center for Structural Biology (CSB)/Univ. of Florida Brain Institute (UFBI)/NHMFL

Microcoils

Mareci, T., UF, CSB/NHMFL
Gibbs, S., NHMFL/FAMU-FSU College of Engineering
Grant, S., Univ. of Chicago
Webb, A., Univ. of Illinois

Work has continued on the microcoil project started last year and funded in part by an NHMFL in-house grant. Several microcoils have been tested and are effective for nanolitre spectroscopy and microimaging. Additionally, a double tuned 1H/23Na microcoil was constructed. Using these coils we have performed two new studies to demonstrate their utility: (1) We have obtained the world's first spatially localized 1H spectra from single neurons. The spectra show osmolytes and metabolites and change with time as cells swell; (2) we have obtained the world's first sodium images of single cells in which the most striking feature is the difference in signal between the cell nucleus and cytoplasm. Both pieces of work are being presented at meetings[1] and written up for publication.

Brain Slices

Buckley, D.L., UF, CSB and UFBI
Bui, J.D., UF
Phillips, M.I., UF

Our NMR studies of isolated perfused brain slices that we imaged for the first time have been continued. A publication describing the effect of the application of ouabain is in press.[2] Preliminary studies on the effects of NMDA (a glutamate receptor agonist) have been completed and a paper is in review.[3] Additionally we have explored the utility of Gd-DTPA in this model as an extracellular marker and have obtained images of the intra and extracellular compartments in the brain slices. This work is also under review.[4] Taken together, these studies establish the brain slice as a useful model for the investigation of the mechanism of MRI signal changes, and we have reviewed these applications.[5]

Major aspects of both these projects have been funded this August by an RO1 (NIH/RO1 NS36992) from the NIH.

References:

1 Grant, S., *et al*., submitted, 40th ENC, Orlando.
2 Buckley, D.L., *et al*., Magn. Reson. Med., in press (1998).
3 Bui, J.D., *et al*., Neuroscience, submitted (1998).
4 Buckley, D.L., *et al*., Magn. Reson. Med., submitted (1998).
5 Bui, J.D., *et al*., *in* "Spatially resolved magnetic resonance" (P. Blumler, B. Blumich, R.E. Botto, E. Fukushima, Eds.), p. 337, Wiley-VCH, Weinheim, (1998); progress report for Dr. S.J. Blackband, 1998.

Radio Frequency Tests of NMR Probe Coils Made of High Temperature Superconducting Materials

Brey, W., Conductus
Withers, R., Bruker
Soble, C., Conductus
Soghomonian, V., NHMFL

We have made, and RF tested, NMR probe coils using high-temperature superconductors (HTS) at fields up to 25 T, corresponding to a proton

frequency of 1.065 GHz. Even at these extremely high fields, the coils demonstrated suitably high quality factors (Q) and sufficiently high current-handling capacities for use in ultra-high-sensitivity high-resolution NMR probes.

The coils were made from thin films of the HTS material $YBa_2Cu_3O_{7-\delta}$, patterned using coil designs developed by Conductus and Bruker. Measurements were made in a resistive magnet at the NHMFL. Coil temperature was maintained at 4.2 K. A 900 MHz coil had a matched quality factor of 25,800 at zero field, which dropped to 22,900 at 21.1 T (900 MHz proton frequency) and 19,900 at 25 T. A 650 MHz coil yielded a Q of 23,900 at fields up to 25 T. The 900 MHz coil carried over 12 amperes of RF current at 21.1 T (sufficient for 90-degree pulses shorter than 10 microseconds), while the 650 MHz coil carried more than 15 amperes at 25 T.

We conclude that HTS materials are suitable for use in ultra-high-sensitivity NMR probes at fields beyond 1 GHz.

This work was sponsored by NSF, Grant No. DMI-9761221.

K_3CrO_8 as a Proposed Standard for g-Factor, Spin Concentration, and Field Calibration in High Field EPR Spectroscopy

Cage, B., NHMFL/FSU, Chemistry
Weekley, A., FSU, Chemistry
Brunel, L.C., NHMFL/FSU, Physics
Dalal, N.S., NHMFL/FSU, Chemistry

Currently, there is a lack of an internal standard for EPR spectroscopy employing magnetic fields higher than about 3 T. Work has been done suggesting that the solid solution of 0.5% K_3CrO_8 into K_3NbO_8 fulfils many of the requirements of such a standard. Its main EPR signal is due to a ($3d^1$) electron, and consists of a single sharp peak for single crystal samples. The peak width[1] ranges from 1.5 G at the X-band (B_o = 0.34 T) to 4 G at 330 GHz (B_o = 11.8 T). The g-values[2] have been determined to a precision of 6 significant figures where $g_\perp = 1.98508 \pm 0.00005$, and $g_{ll} = 1.94272 \pm 0.00005$. This high degree of precision is necessary because EPR work at high frequencies can resolve g-tensors to six and seven significant figures. Additionally, K_3CrO_8 provides a field calibration standard[3] via a weak, but well resolved hyperfine structure from its ^{53}Cr isotope (I=3/2, natural abundance 9.5%): $A_{ll} = 39.55 \pm 0.08$ G, $A_\perp = 11.49 \pm 0.05$ G. Variable temperature and variable frequency measurements demonstrate that this sample can serve as a reliable standard for EPR measurements over the range of at least 5 K to 300 K and 9 GHz to 330 GHz, respectively. The sample can be prepared in a simple, reproducible way, and can serve also as a standard for absolute spin count, thus making it unique among the other standards in current usage. Table 1 lists the various advantages and disadvantages of common EPR standards.

Table 1. Comparison of various EPR standards.

	0.5% K_3CrO_8/K_3NbO_8	Mn(II) in MgO	DPPH
Concentration Standard	Absolute spin measurements possible	Not possible	Not possible
Purity	Easily synthesized in pure form	Difficult high temperature synthesis	Difficult
g-Value Precision	±0.00005 Good for g < 2 and also good for g = 2	±0.00005 May overlap g = 2 signals, second order effects	±0.0002 May overlap g=2 signals, and lineshape is sample dependent
Field Linearity	Possible via hyperfine. Also possible via two g-values	Second order hyperfine complications	Not possible
Temperature Dependence	Curie law intensity. Lineshape, hyperfine g-value constant	Lineshape temperature dependent	Phase transition at 30 K Significant temp. dependent line broadening

References:

1 Cage, B., *et al.*, J. Magn. Reson., 135, 178-184 (1998).
2 Cage, B., *et al.*, Anal. Chem, submitted (1998).
3 Dalal, N.S., *et al.*, Anal. Chem., 53, 938-940 (1981).

Determination of Gramicidin Channel Structures in Hydrated Phospholipid Bilayers by Solid State NMR

Cotten, M., NHMFL/FSU, Chemistry
Fu, R., NHMFL
Cross, T.A., NHMFL/FSU, Chemistry

In the intricacy of the three-dimensional (3D) arrangement of biologically active molecules lie unique, distinctive structural features that are subtly related to function. Accurate structural determination is therefore crucial to structure-function relationships, but there are no straightforward methods to study membrane bound species with solid-like properties. Solid state NMR has been widely applied to membrane inserted polypeptides such as gramicidin. Gramicidin A, a 15-amino acid polypeptide forms dimeric cation-selective channels in lipid bilayers and is often used as a model for ion channels. Amino acid side chains are believed to mediate key protein-lipid interactions and thereby to play important roles in function. The aromatic, amphipathic side chain of tryptophan (Trp) is a very versatile amino acid in membrane proteins and the focus of our study has been on the structural role of the four tryptophans of gramicidin A.

Gramicidin M (gM) in which all Trp is substituted by aromatic, non-polar phenylalanine (Phe) is used as a model in order to get some insight into the structural conversion for which it is speculated that gA is inserted as a double stranded dimer and then unscrews to form a single stranded channel rather than inserted as monomers that dock to form the channel. Previous studies[1] indicated that gM feature a left-handed double stranded dimer structure in lipid bilayers. In this work, a double-labeled ^{13}C and ^{15}N gM (Alanine$_5$-$^{13}C_1$, phenylalanine$_{11}$-^{15}N) was incorporated into hydrated lipid bilayers and the distance constraint between these two sites was determined by a newly developed simultaneous frequency and amplitude modulation (SFAM)[2] that is capable of detecting weak interactions in solid state magic angle spinning (MAS) NMR, allowing to determine the gM dimer structure. As illustrated in Figure 1, the SFAM distance measurement confirms that the dimer is antiparallel. The combined use of orientational and distance constraints is shown to be a powerful structural approach.

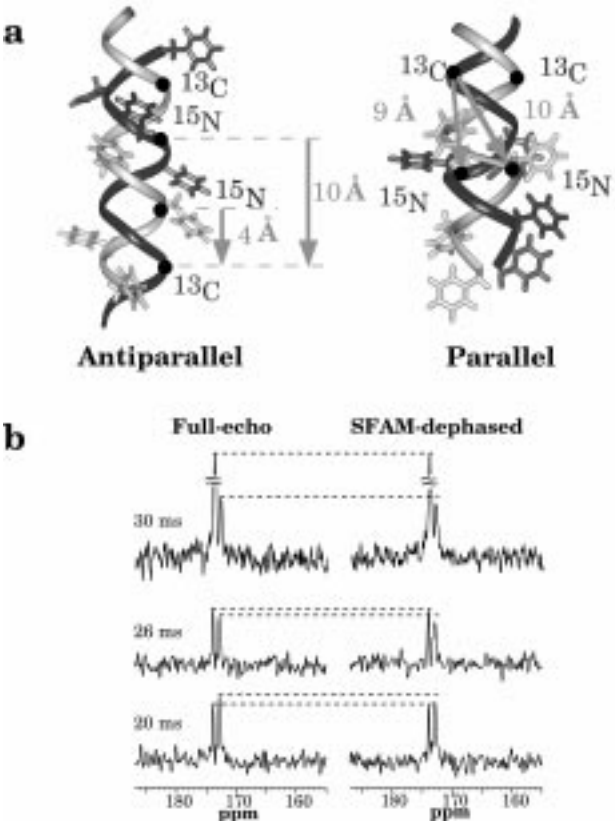

Figure 1. (a) Two possible dimer structures of gramicidin M in hydrated DMPC bilayers. The solid circles indicate the labeled sites of ^{13}C and ^{15}N. (b) A set of ^{13}C CPMAS spectra at different dephasing times with (left) and without (right) the SFAM irradiation on the ^{15}N channel. The spectra were recorded at 315 K (above the phase transition temperature of DMPC) on a Bruker DMX 300 NMR spectrometer. The peak at 174 ppm is not affected by dephasing and is therefore assigned to the carbonyl group of the lipids. The peptide resonance at 173 ppm is attenuated by the SFAM irradiation, indicating a residual dipolar coupling of 19 ± 3 Hz. Taking into account the orientation of the internuclear $^{13}C/^{15}N$ vector with respect to the global motion axis, the distance between the ^{13}C-^{15}N pair is 4.5 ± 0.3 Å, consistent only with the antiparallel dimer structure.

References:

1 Cotten, M., *et al.*, Biophys. J., 73, 614 (1997).
2 Fu, R., *et al.*, Chem. Phys. Lett., 272, 361 (1997).

The Use of PFG-NMR for the Measurement of Diffusion Coefficients of the *Cis* and *Trans* Isomers of Proline-Containing Peptides

Derrick, T., Univ. of Kansas, Chemistry
Larive, C.K., Univ. of Kansas, Chemistry

Tiffany Derrick, a Ph.D. candidate in my research group at the University of Kansas, and I (CKL) visited the NHMFL for one week during March, 1998. During our visit we used the 720 MHz NMR spectrometer primarily for measurements of diffusion coefficients of proline-containing peptides. Although we had performed some measurements on our 400 MHz spectrometer at the University of Kansas, one of the peptides, arginine vasopressin, had a sufficiently complex spectrum and low cis isomer content (6%) that the analysis required the increased dispersion and sensitivity of a higher field instrument. A manuscript including the data obtained at the NHMFL titled *The Use of PFG-NMR for the Measurement of Diffusion Coefficients of the Cis and Trans Isomers of Proline-Containing Peptides* (T. Derrick and C.K. Larive) was submitted to Magnetic Resonance in Chemistry on October 26, 1998. The NHMFL and the help of Dr. Murali are acknowledged in this manuscript.

While at the NHMFL, we also ran some 2D NMR experiments and attempted an FT-ICR analysis of a small copper-binding compound isolated from methanotrophic bacteria. Although these experiments did not produce publishable results, they did provide some information that was useful in our ongoing research effort in this area.

High Zeeman Field Narrowing of the NMR Peaks of Spin 1/2 Nuclei Coupled to Quadrupolar Nuclei: ^{31}P NMR Widths as a Probe of the $RbH_2PO_4(x)$-NH_4 $H_2PO_4(1-x)$ Proton Glass

Fu, R., NHMFL
Dalal, N.S., NHMFL/FSU, Chemistry

The understanding of the microscopic origin of the electric analog of the spin glass behavior by a random mixture of a single crystal of a ferroelectric and an antiferroelectric lattice is one of the areas of active research in phase transitions. In particular, this opens up a new area in solid state physics wherein one can compare the fundamental similarities and differences between a behavior of the magnetic dipoles versus electric dipoles. It has now been well established that in a certain composition range, the mixed crystals of the ferroelectric compound RbH_2PO_4 (RDP) and $NH_4H_2PO_4$ (ADP) exhibit a spin glass behavior,

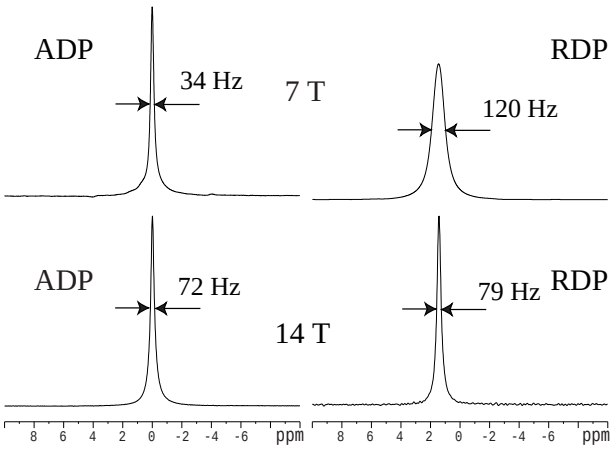

Figure 1. ^{31}P CPMAS NMR spectra of ADP and RDP at different fields. The ^{31}P linewidth of ADP at high field was broader than at low field because of the magnetic susceptibility effect. For RDP, however, the ^{31}P linewidth was broader at low field. No line broadening factor was applied during the data processing.

but the details of the underlying mechanism are still not fully understood.

In order to obtain new clues to this phenomenon, we have initiated a systematic study of the utility of the high field NMR techniques. We have carried out ^{31}P NMR measurements on a series of RDP(x) ADP(1-x) compositions. It is found that high field NMR affords a significant enhancement in both sensitivity and resolution of a spin-1/2 nucleus coupled to quadrupolar nuclei of half-integer spin in the case of the Rb dominated compositions, as shown in Figure 1, owing to the attenuation of the second-order quadrupolar interactions at high field that significantly contribute to line broadening. By suppressing this effect, high field NMR allows us to study the line broadening that results from nature of the glass-like behavior in systems, thus opening up a new avenue for studying these so-called proton glasses. Such work cannot be done at low field where the quadrupolar contributions to linewidths hinder such studies.

Temperature-Jump 2D NMR Spectroscopy in Crystalline Solids: A Technique for Correlating Molecular Reorientation Across the Phase Boundaries of an Order-Disorder Lattice

NHMFL

Fu, R., NHMFL
Bodenhausen, G., Ecole Normale Supérieure, France
Dalal, N.S., NHMFL/FSU, Chemistry

In this report, we describe a two-dimensional high resolution solid state NMR methodology for correlating the dynamics of molecular rearrangements around the critical points of equilibrium phase transitions in molecular solids.[1] It combines the techniques of temperature-jump and two-dimensional (2D) NMR spectroscopy. The two spectral dimensions are the isotropic chemical shifts at different sample temperatures. The technique is illustrated by elucidating the dynamic rearrangement of the C_4O_4 units of squaric acid ($H_2C_4O_4$) in relationship to the mechanism of its antiferroelectric phase transition at $T_N \sim 373$ K. These results clarify the apparent discrepancy between the conclusions derived earlier from NMR, X-ray, and Raman and neutron scattering studies, as shown in Figure 1. They were a direct consequence of the significant enhancement in the NMR spectral resolution through this technique, which thus might prove to be a significant new aid in understanding the mechanisms of phase transitions in molecular solids.

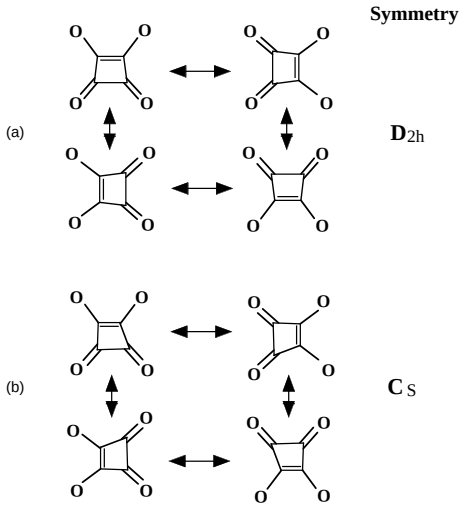

Figure 1. Possible structures of the high temperature forms of squaric acid: (a) regular trapezoid, and (b) irregular trapezoid. The H's are omitted for the sake of clarity. The present study supports the geometrical form represented in (b).

This research is related to In-House Research Program, Project #5017.

Reference:

1 Fu, R., *et al*., J. Phys. Chem., B102, 8732 (1998).

Polarization Transfer in Multiple-Spin Systems and High Resolution NMR Dipolar Spectroscopy of Oriented Solids

Gan, Z., NHMFL

Measurement of nuclear spin dipolar coupling directly yields distance and orientation information for structural determination of solids. For oriented samples, dipolar coupling can be measured using the separated-local-field (SLF) experiment[1] that spreads dipolar coupling by chemical shift in a two-dimensional (2D) spectrum. Recently, NMR technique based on polarization transfer, particularly the Polarization Inversion Spin-Exchange at the Magic-Angle (PISEMA) experiment,[2] greatly improves spectral resolution over the conventional SLF experiment. The spectra of methyl-α-D-glucopyranoside single crystal in Figure 1 demonstrate the resolution improvement by PISEMA.

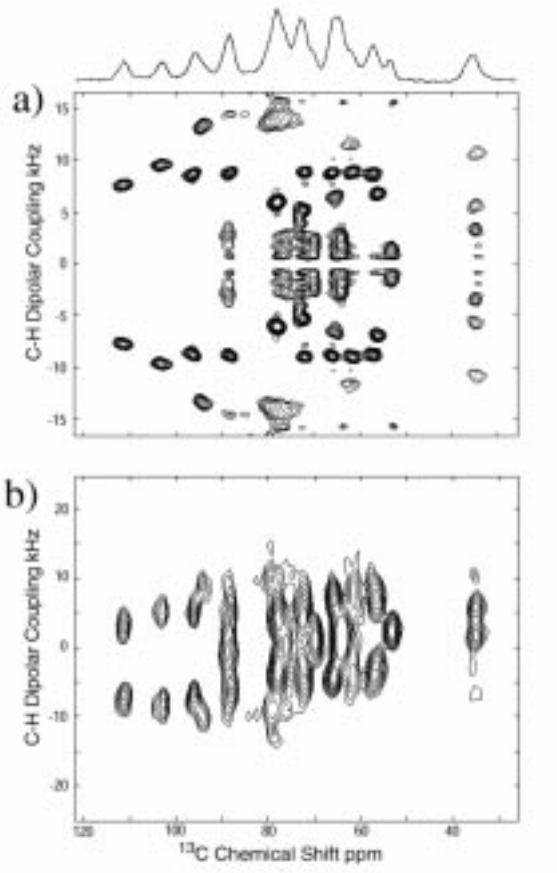

Figure 1. a) 2D PISEMA and b) 2D SLF spectra of methyl-α-D-glucopyranoside single crystal at arbitrary sample orientation.

As illustrated in Figure 2, the origin of this resolution improvement comes from the fact that PISEMA removes the broadening from long-range dipolar coupling of remote spins. In a SLF experiment, long-range dipolar coupling causes multiplet patterns in the dipolar spectrum and it effectively makes the spectral line broad. In a PISEMA experiment, however, the dipolar spectra is obtained from the transient oscillation of polarization transfer and both theory and numerical simulation show that the presence of remote spins only perturbs the polarization transfer between two directly bonded spins. Therefore, the linewidth of the resulting dipolar spectrum remains unaffected by the long-range dipolar coupling in the PISEMA experiment.

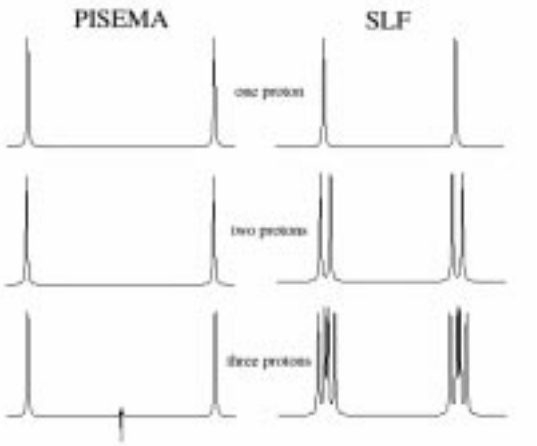

Figure 2. PISEMA (left) and SLF (right) dipolar spectra calculated for a ^{13}C spin coupled to one, two, or three protons. The ^{13}C-^{1}H dipolar coupling are 20, 1.5, and 1.0 kHz, respectively.

References:

1 Waugh, J.S., Proc. Natl. Acad. Sci. USA, 73, 1394 (1976).

2 Hu, C., *et al*, J. Magn. Reson. A, 109, 270 (1994).

Magnetic Resonance Evaluation of Spinal Cord Injury

Mareci, T.H., NHMFL/UF, Biochemistry
Inglis, B.A., NHMFL/UF, Neuroscience
Silver, X., UF, Biochemistry
Mercer, E., UF, Biochemistry
Bossart, E.L., UF, Physics
Wirth, E.D., UF, Neuroscience

Implanted ^{31}P RF coils. We have designed and implemented an inductively-coupled, implantable ^{31}P RF coil[1] for the study of spinal cord metabolism *in vivo*. This coil was employed to obtain the first *in vivo* ^{31}P localized NMR spectra from a rat spinal cord using a chronically implanted inductively driven coil. A 4 x 5 mm inductively coupled coil with a resonance block circuit was coated with a bio-compatible acrylic, and implanted above a T-13 vertebral level laminectomy. The implanted coil's resonance block circuit allowed decoupling during RF transmission, and optimal coupling to a 3 x 3 cm surface coil during reception. RF field excitation was thus achieved solely by the external surface coil, which was mounted on a Plexiglas cradle designed to support a supine rat. This design scheme provided uniform magnetic field excitation and a highly sensitive, chronically endured, inductively coupled implanted reception coil. As the localization accuracy of the implanted coil system alone is inadequate and permits contamination from surrounding tissues, a gradient pulse sequence was employed to localize to a 1.25 x 1.00 x 5.85 mm (7 μL) voxel within the spinal. The resulting spectra had a SNR of approximately 3.5 to 1 with a PCr to β-ATP ratio of 2.4 to 1.

Using the combination of coil design and pulse sequence localization, the obtained ^{31}P spectra demonstrated metabolite ratios indicative of healthy spinal cord tissue, and showed no contamination from surrounding tissues. Furthermore, the application of inductively coupled implantable coils induced no adverse reactions in the rat, thus validating the potential for long term longitudinal studies. Using this methodology, changes in spinal cord metabolism can be monitored periodically with optimal sensitivity and no contamination from adjacent tissues.

In vitro measurement of anisotropy water diffusion in spinal cord cellular compartments. We have used high magnetic field gradient weightings to measure, for the first time, multiple-component diffusion tensor images in excised, fixed central nervous system tissue.[2-4] This work involves two *in vitro* studies: one using spectroscopy on a sample of excised, fixed human corpus callosum, and a second using an imaging sequence on a sample of excised, fixed rat spinal cord. Only two unique components of diffusion were observed for the limits of the gradients utilized (~10000 s/mm^2). The spectroscopy data was fit as a full biexponential diffusion matrix, and fit very well to an anisotropic biexponential model. The imaging data was fit pixel-wise to the full biexponential diffusion model to get a full tensor of directional information in both the fast and slow diffusing regimes. These results can be interpreted in terms of extracellular (fast) and intracellular (slow) diffusion within the CNS tissue. This is the first measurement of biexponential diffusion tensor imaging, and provides a novel view of tissue morphology representative of organization at the intra- and extracellular level in the spinal cord.

References:

1 Ni, W.X., *et al*., Proc. Int. Soc. Mag. Reson. in Medicine, Sydney, Australia, April 18-24, 1998.
2 Bossart, E.L., *et al*., Proc. Int. Soc. Mag. Reson. in Medicine, Sydney, Australia, April 18-24, 1998.
3 Inglis, B.A., *et al*., Proc. Int. Soc. Mag. Reson. in Medicine, Sydney, Australia, April 18-24, 1998.
4 Inglis, B.A., *et al*., accepted for publication in Am. J. Neuro. Rad., 1998.

Formulation and Demonstration of a New Mass Spectral Line Shape for High-Mass Trapped Ions

Marshall, A.G., NHMFL/FSU, Chemistry
Guan, S., NHMFL/FSU, Chemistry
Li, G.-Z., NHMFL
Bossio, R.E., FSU, Chemistry
Vining, B.A., FSU, Chemistry

The decay amplitude envelope of an ICR time-domain signal determines its corresponding Fourier transform mass spectral line shape. The commonly accepted FT-ICR frequency-domain unapodized Lorentzian spectral line shape originates from the Langevin ion-neutral collision model (a point-charge ion induces an electric dipole moment in a neutral collision partner). The Langevin model is a good description for reactions of low energy collisions of low mass positive ions with neutrals. However, the Langevin model is inappropriate for collisions of high-mass gas-phase biopolymer ions with low-mass neutrals.

For the Langevin model, collision frequency is independent of ion speed, leading to a linear differential equation of ion motion with a frictional damping term linearly proportional to ion velocity. For the hard-sphere model, collision frequency is proportional to ion speed and the frictional damping term is proportional to the *square* of ion velocity. The resulting (non-linear) equation of ion motion leads to a non-exponential time-domain ICR signal whose amplitude envelope has the form, $1/(1 + \delta t)$, in which δ is a constant.

We have demonstrated the new line shape experimentally in three ways: (a) direct fitting to the theoretical shape; (b) dispersion vs. absorption (DISPA) line shape analysis; and (c) mass resolving power enhancement for pressure-limited absorption-mode over magnitude-mode line shape: experimental enhancement factor of 1.43 ± 0.09 for isotopically resolved FT-ICR mass spectra of electrosprayed bovine carbonic anhydrase (~29 kDa), compared to theoretical factors of 1.40, and for hard-sphere and Langevin, respectively.[2]

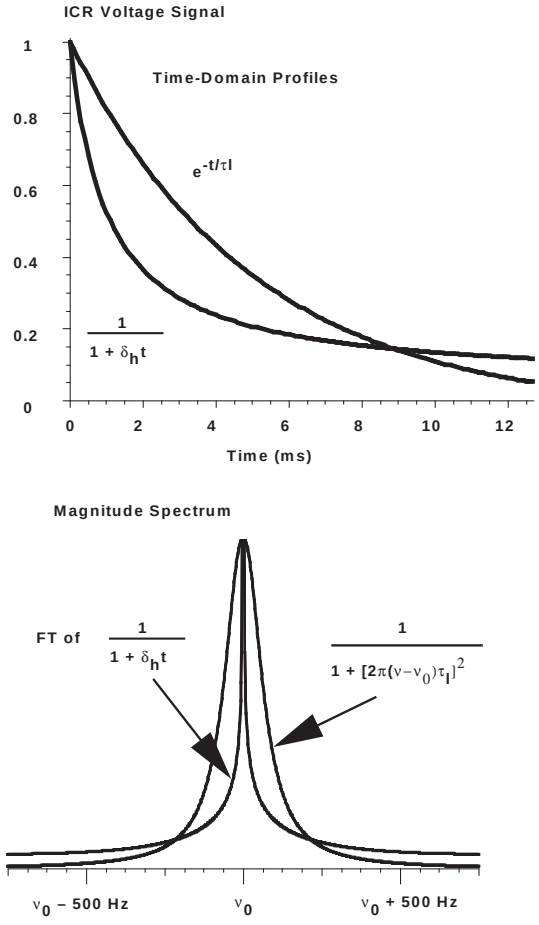

Figure 1. Time domain profiles (top) and frequency-domain magnitude-mode positive-ion spectra (bottom) of ion cyclotron signals simulated from Langevin and hard-sphere ion-neutral collision mechanisms.

References:

1 Guan, S., *et al*., Int. J. Mass Spectrom. Ion Proc., 167-168, 185-194 (1998).
2 Vining, B.A., *et al*., Anal. Chem., 70, (1998).

High Field EPR Experiments in the Compound $La_2Ni_{0.5}Li_{0.5}O_4$

NHMFL

Pagliuso, J.P., UNICAMP, Brazil
Rettori, C., UNICAMP, Brazil
Oseroff, S., San Diego State Univ., Physics
Sarrao, J., LANL
Hassan, A., NHMFL
Martins, G.B., NHMFL
Fisk, Z., NHMFL
Brunel, L.C., NHMFL

High field EPR measurements were performed in powdered samples of $La_2Ni_{0.5}Li_{0.5}O_4$ to complement thermodynamic measurements such as magnetic susceptibility and x-ray. Previous Raman scattering experiments were also performed. The compound is supposed to undergo a Jahn-Teller distortion because the strength of the crystal field in the Ni site induces a high-spin configuration in the Ni^{3+} ion, which is known to be Jahn-Teller active. We believe that the temperature dependent variation of the g factors (perpendicular and parallel) of the Ni could be indicative of some dynamic Jahn-Teller effect. Right now we are in the process of explaining such $g \times T$ variation through a Jahn-Teller mechanism.

This work was supported by an NHMFL In-House Research Program grant.

Understanding Dispersion in Chromatography

Park, J.K., NHMFL/FAMU-FSU College of Engineering
Whittenberger, F., FAMU-FSU College of Engineering
Shine, J., FAMU-FSU College of Engineering
Gibbs, S.J., NHMFL/FAMU-FSU College of Engineering

Work continued on characterizing non-uniform flow and dispersion in packed columns used for chromatographic separations.

Bulk displacement spectra (or propagators) and spatially resolved velocity and dispersion maps have been obtained for fluid flow in packed beds of impermeable and permeable particles by Fourier (or q-space) magnetic resonance flow imaging. Typical displacement spectra, showing fluid element displacements as a function of time allowed for flow, for selected slabs of an entire packed column cross section, are asymmetric for short displacement times, and approach a Gaussian shape at long displacement times. The short-time spectra reflect the instantaneous distribution of fluid velocities in the interstiticies between packing particles. These asymmetric spectra are averaged to Gaussian shapes by transverse diffusion and dispersion. Examples are shown in Figure 1.

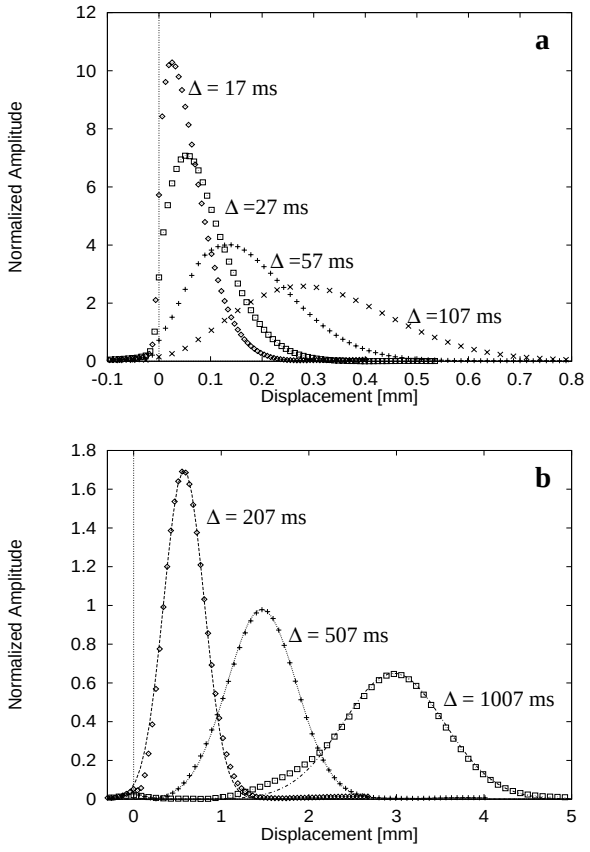

Figure 1. Displacement spectra (or propagators) for the flowing fluid in a packed bed of impermeable polystyrene spheres (99 μm diameter) for a range of evolution times. Note that the spectra are nearly Gaussian for long evolution times in (b). Points are experimental data obtained with an APGSTE NMR sequence for a 5 mm thick slice through an 11.7 mm diameter packed column.

Spatially resolved fluid velocity maps over column cross sections have been obtained by Fourier (or q-space) magnetic resonance flow imaging. For axially compressed beds of impermeable particles, the velocity distributions are radially non-uniform with the largest velocity near the column center, and the smallest velocity about three particle diameters from the column wall. An example is shown in Figure 2.

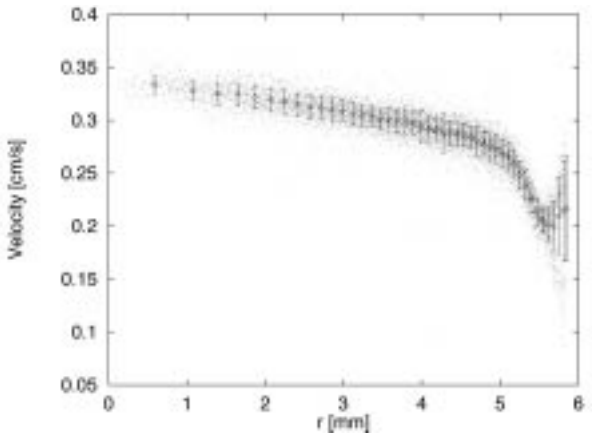

Figure 2. Radial dependence of fluid velocity in an 11.7 mm diameter column packed with 99 μm diameter polystyrene beads determined from analysis of APGSTE MRI data. Note that the velocity field is systematically radially nonuniform.

Work is underway to quantitatively model transverse dispersion and its effects on observed flow non-uniformity in macroscopic measurements, and to perform similar measurements on fluidized beds.

Magnetic Resonance Imaging of Liquid Flow in Porous Materials Containing a Transverse Permeability Discontinuity

NHMFL

Pavlovskaya, G.E., NHMFL
Gibbs, S.J., NHMFL/FAMU-FSU College of Engineering

Viscous fluid flow in porous media is important in many disciplines including biology and medicine, ground-water and soil science, reaction and petroleum engineering, separation science, waste treatment, heat transfer, and composite manufacturing. An important aspect of these flows that remains intractable is the compact description of viscous fluid behavior at a transverse interface between a free liquid and a saturated porous medium. Magnetic resonance imaging velocimetry allows spatially resolved measurements of fluid velocities in bulk liquids, porous media, and near the interface between the two,[1] and has been used for the determination of apparent slip velocities.[2]

We have applied MRI velocimetry techniques to study flow behavior in a 23 mm OD diameter sponge-like material with an average pore size of 2 mm, and a cylindrical channel of 7 mm diameter cut through it. Spin-echo MRI measurements allow detailed study of the flow in the central open channel, and stimulated echo measurements have been designed to determine temporally averaged flow in the porous material. Two dimensional images were acquired in 128 x 128 pixels for a spatial resolution of approximately 200 μm. Analysis of the resulting velocity fields allowed determination of deviation from pure Darcy flow in the porous material and of apparent slip velocities in the open channel (see Figure 1). Work will continue through the study of flow development in the two regions, and by comparing measured deviations from pure Darcy flow with various theoretical predictions.

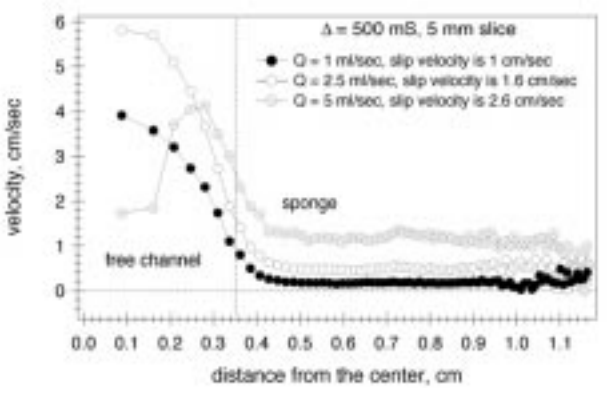

Figure 1. Radial velocity profiles in porous sponge with a central open channel showing non-zero apparent slip velocities for all flow rates studied.

References:

1 Vasanathan, R., *et al.*, Magnetic Resonance Imaging, 13 (5), (1995).
2 Gibbs, S.J., *et al.*, J. Rheol., 40 (3), 425-440 (1996).

Relaxation Effects in a System of a Spin-1/2 Nucleus Coupled to a Quadrupolar Spin Subjected to RF Irradiation: Evaluation of Broadband Decoupling Schemes[1]

Smith, S.A., NHMFL
Murali, N., NHMFL

We have investigated the suitability and performance of various decoupling methods on systems in which an observed spin-1/2 nucleus I (^{13}C or ^{15}N) is scalar-coupled to a quadrupolar spin S (^{2}H). Decoupling of these systems can be critical to the success of some protein NMR experiments. For example, deuterium labeling is often used on proteins to quench ^{13}C-^{1}H dipolar interactions with the hope of improving their ^{13}C NMR spectra *via* line narrowing (from reduced dipolar relaxation.) Unfortunately, quadrupolar relaxation from ^{2}H can result in ^{13}C transitions that are even broader than those of the unlabelled protein. This undesirable broadening is more likely to occur in larger molecules and at high fields, *i.e.* on the biomolecules of interest in the optimal spectrometers (where spectral dispersion is largest). Decoupling can effectively eliminate such broadening and allow experimentalists to regain the line-narrowing benefits of ^{2}H substitution in proteins at high fields. A key aspect in protein decoupling is to avoid sample heating (which can destroy the sample) by using minimal rf-power while still achieving the necessary decoupling level.

Experiments on the 720 MHz NMR spectrometer at the NHMFL have been conducted by varying the strength of the irradiating radiofrequency (RF) field, RF offset, relaxation times, and decoupling schemes applied in the vicinity of the S-spin resonance. In addition, simulations of these and other experiments have been carried out using the GAMMA platform. The T_1 relaxation of the quadrupolar spin has previously been shown to influence the efficiency of the continuous wave (CW) decoupling applied on resonance in such spin systems.[2] Similarly, the performance of broadband decoupling sequences should also be affected by relaxation. Virtually all of the more commonly used broadband decoupling schemes, however, have been developed without consideration of relaxation effects. As a consequence, it is not obvious how one selects a suitable sequence for decoupling quadrupolar nuclei with exotic relaxation behavior. We have demonstrated that, despite its simplicity, WALTZ-16 decoupling is relatively robust under wide range

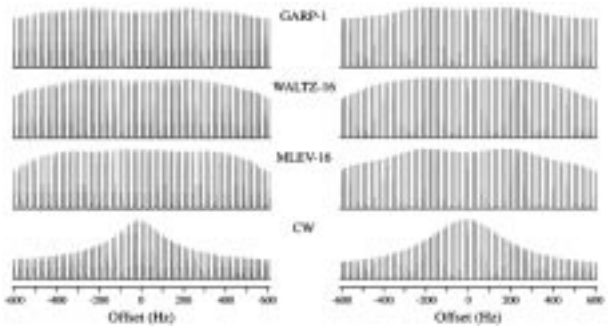

Figure 1. Experimental (left column) and simulated (right column) 180 MHz ^{13}C (720 MHz ^{1}H) spectra of the ^{13}C-^{2}H portion of glycerol-d8 *vs.* ^{2}H decoupler offset. The decoupler rf-amplitude was set at 435 Hz. A total of 61 offsets were taken in increments of 20 Hz. The plotted range on each was 300 Hz centered about the ^{13}C shift. Experimental: The spectral width was set to 11500.9 Hz and 16 K points taken per offset. The data was zero filled to 64 K and a 2.0 Hz line broadening applied prior to Fourier transformation. The experimental sample temperatures and simulation correlation times are -10 °C and 1.0 ns respectively. Additional simulation parameters were J(^{13}C-^{2}H) = 22 Hz, r(^{13}C-^{2}H) = 1.09 Å, CSA(^{13}C) = 100 PPM, QCC(^{2}H)=175 KHz. For simplicity the asymmetry values were set to zero. Although their relative orientations do affect the lineshapes, they had little effect on the simulated decoupling profiles.

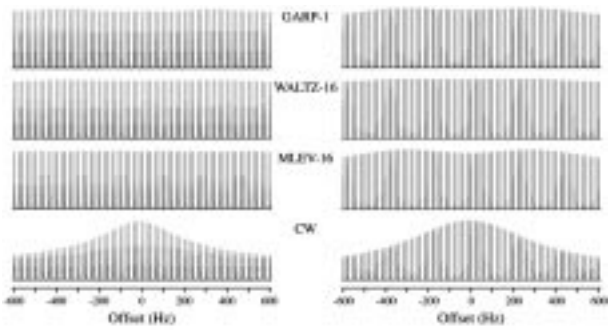

Figure 2. Experimental (left column) and simulated (right column) 180 MHz ^{13}C spectra of the ^{13}C-^{2}H portion of glycerol-d8 *vs.* ^{2}H decoupler offset. The decoupler rf-amplitude was set at 686 Hz. All other parameters were identical to those specified in Figure 1.

of decoupling conditions. In these systems it performs as well as the more recently developed decoupling schemes for wide band-width applications such as GARP-1 and CHIRP-95. It has been found that (Figures 1 and 2), in macromolecular motional regimes, broadband deuterium decoupling can be achieved with relatively low RF amplitudes (500-700 Hz) using WALTZ-16 multiple pulse decoupling.

References:

1 Smith, S.A., *et al*., J. Magn. Reson., 135, in press, 1998.
2 Murali, N., *et al*., J. Magn. Reson., A 118, 202-213 (1996).

STRAFI: A GAMMA Investigation

Smith, S.A., NHMFL
Randall, E.W., Queen Mary & Westfield College, London

STRAFI (STRAy Field Imaging) is an NMR technique that takes advantage of the strong field gradients existing in the immediate vicinity *outside* a spectrometer's magnet. As in other imaging methods, the gradient promotes a spatial separation of resonance frequencies throughout a sample thus allowing an experimentalist to selectively probe particular sample areas. Larger gradients produce larger spatial frequency separations and generally enhance image resolution, and the gradients in STRAFI (~50 T/m) are very large. Furthermore, STRAFI employs a modified Hahn echo sequence (Figure 1), typically a $90_{\phi} - (\tau - 90_{y} - \tau)_{n}$. Using STRAFI, echoes have been observed for a wide variety of both solid and liquid samples. Such broad applicability is one of several reasons STRAFI is such a useful tool for imaging & materials characterization.

Aside from its proven applicability, there are several aspects of STRAFI that demand further investigation. Basis questions regarding experiment parameter optimization remain unanswered and there is a distinct possibility that a refined echo analysis would be a source of additional sample information. Since all but primitive theoretical treatments are tenable, we have used computer simulations to explore these and other areas. A module supporting magnetic resonance simulations in gradients has been added to the GAMMA simulation platform. GAMMA, supported at the NHMFL and used worldwide, now additionally serves as a general tool for STRAFI calculations.

One of the first STRAFI issues addressed with GAMMA was pulse sequence optimization. Pulse calibration can be problematic in stray field experiments. Simple theory indicates that given a specific pulse length maximum echo amplitudes will be observed for an on-resonance angle of 90° degrees whereas given a specific field strength the maximum would be observed for a 120° pulse angle. GAMMA calculations have demonstrated that this is NOT strictly true. For typical pulse strengths and lengths we observe that the maxima

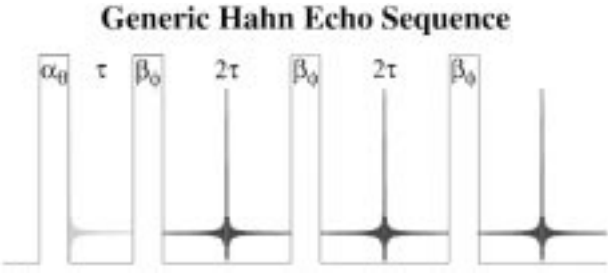

Figure 1. Hahn echo sequence. Echoes shown result from the sequence 90_{x}–$(\tau$–90_{y}–τ–$)_{n}$.

are significantly off of the "ideal" values. Indeed, when one samples the echo intensity over a range of pulse lengths and strengths it becomes evident that the echo maxima vary depending upon the type of pulse applied. An interesting result is that Gaussian 120° pulses consistently maximize the echoes over a wide range of lengths and strengths (Figure 2).

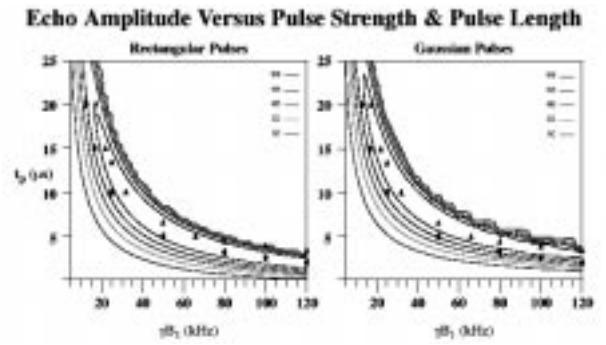

Figure 2. Simulated intensities of the first STRAFI echo over differing RF field strengths and pulse lengths for the odd echo sequence. The dots indicate where 90° pulses would be and the triangles indicate 120° pulses. The system was a single proton in a 50 T/m gradient. The effective system length 10 μm, 3000 sub-systems were used and the base field strength set to 300 MHz. Rectangular pulses were used in the contour map on the left. Gaussian pulses (101 steps, 2% endpoint cutoff) were used in the contour map on the right.

In STRAFI work the phase of the initial pulse relative to the subsequent pulse train has a dramatic effect on the echo amplitudes. The *odd sequence* $90_x - (\tau - 90_y - \tau)_n$ produces echoes which are all positive whereas echoes from the *even sequence* $90_y - (\tau - 90_y - \tau)_n$ oscillate between positive and negative intensities. In small field-gradients solid compounds containing spin 1/2 nuclei produce *dipolar echoes* if the *odd* sequence, $90_x - \tau - 90_y$, is applied but NOT following the *even* $90_x - \tau - 90_x$ sequence. This contrasts with experiments performed in very large gradients (~50 T/m) where either sequence will produce *Hahn echoes* from both solids and liquids (for any pulse angle). The general expectation is that two pulses will produce one echo, but in fact many echoes can be obtained. In order to understand the relationship between *Hahn echoes* and gradient strength relative to *dipolar echoes* we have used GAMMA to simulate these two echoes. Figure 3 illustrates the disappearance of the dipolar echoes while the Hahn echoes appear as the gradient increases. The dipolar echo is washed out by dephasing effects caused by the gradient.

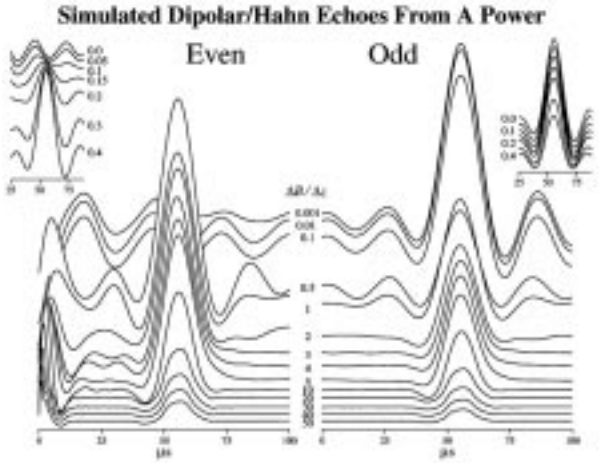

Figure 3. Simulated echoes versus gradient strength following $90_{x,y}$–τ–90_y. The system consisted of two protons set to resonance at 300 MHz with a 50 KHz dipolar coupling. The pulses were rectangular and of 10 μs length, and the delay was set to 50 μs. A 2 KHz apodization was applied and powder averaging included in the calculation. The inset scans show the critical gradient strengths where Hahn echoes compete with dipolar echoes.

Much of this work was presented at the 1998 Ampere Conference.

The Keck Magnet and NMR Applications

Soghomonian, V., NHMFL
Cross, T.A., NHMFL/FSU, Chemistry

Spurred by the need for higher field strengths in the area of magnetic resonance, and the NHMFL's successes in generating moderately homogeneous, very high fields, the Keck Foundation generously supported the development of a 25 T (1066 MHz ^{1}H frequency), 52 mm bore magnet.

The Keck magnet is constructed from 3 concentric Bitter stacks. The middle stack is electrically shorted at the center to produce a relatively homogeneous region in the magnetic field profile. The on-axis, as well as the off-axis, profiles were generated by NMR measurements, represented in Figure 1. These maps were obtained by moving a 2 mm diameter spherical sample of D_2O, and recording the variations of the resonance frequency of the deuterium signal. The NMR probe is attached to a threaded rod that provides a 1.27 mm vertical displacement corresponding to every 360 degree rotation. A data point is collected for every full rotation with a sample placed along the vertical Z axis resulting in the on-axis map. To map the variations in the magnetic field in the radial X and Y planes, the same sample was placed 5 mm off the Z axis. Data in this case was collected at every 74 degrees. The combined information available from these two maps is used for (a) choosing the optimal position in the magnet for experiments, and (b) designing correction coils to reduce the spatial inhomogeneities. The spatial homogeneity over a 2 mm diameter spherical sample of D_2O is 3 ppm. We aim to achieve a 1 ppm peak to peak variation over a spherical volume of 10 mm diameter with a combination of passive and active shim sets. The temporal stability of this magnet, with only flux stabilization, is 2 ppm peak to peak over extended periods. From our previous results,[1] we extrapolate that the addition of a field frequency lock will further reduce the temporal variations by an order of magnitude. The spectrometer attached to this magnet for NMR applications is an in-house modified Tecmag system, providing H-X capabilities.

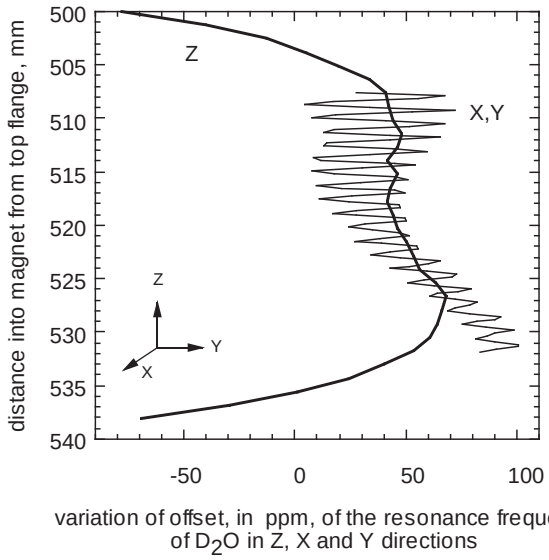

Figure 1. Variation of the NMR offset as a function of position.

A range of novel NMR experiments in chemistry and biology become accessible at the highest proton frequency available, given a magnet with 1 ppm spatial homogeneity and a fraction of 1 ppm temporal stability.

Reference:

1 Soghomonian, V., *et al*., J. of Mag. Reson., 125, 212 (1997).

^{13}C Selective Polarization and Spin Diffusion in a Lipid Bilayer Bound Polypeptide by Solid-State NMR

Tian, F., NHMFL/FSU, Chemistry
Fu, R., NHMFL
Cross, T.A., NHMFL/FSU, Chemistry and Molecular Biophysics

The development of solid state NMR as a protein structural method is facing a significant challenge: the assignment of resonances from uniformly labeled samples. The successful structural characterization of the polypeptide, gramicidin A, was accomplished with single site labeling. This becomes impractical, however, for much larger molecular structures, where it is necessary to incorporate multiple labels simultaneously. A family of NMR experiments derived from PISEMA, are available for resolving many resonances, but methods have yet to be developed for assigning the individual resonances to specific sites within the molecular structure. Several approaches are being pursued; most of which are dependent on spin diffusion between neighboring sites. Unfortunately, this process is very slow

between adjacent ^{15}N labeled sites requiring as much as 3 or 4 seconds to gain significant spin exchange. Since this is on the order of the T_1 relaxation time the signals are very weak from a nucleus that generates weak signals in the first place.

Here, we have initiated experiments on ^{13}C labeled samples. ^{13}C has numerous disadvantages even though it is a more sensitive nucleus than ^{15}N. Carbon is much more common than nitrogen, and the natural abundance of ^{13}C is also greater than that of ^{15}N, therefore, natural abundance signals in ^{13}C spectra represent a much bigger problem than in ^{15}N spectra. Furthermore, in studies of the protein backbone, carbon is bonded to nitrogen, and when the sample is not ^{15}N labeled, the ^{13}C sites are bonded to the quadrupole nucleus, ^{14}N. The dipolar interaction between ^{13}C and ^{14}N can lead to broad resonances and undesirable relaxation properties. ^{13}C has an important advantage, however: spin diffusion rates are much more rapid than the T_1 relaxation rates.

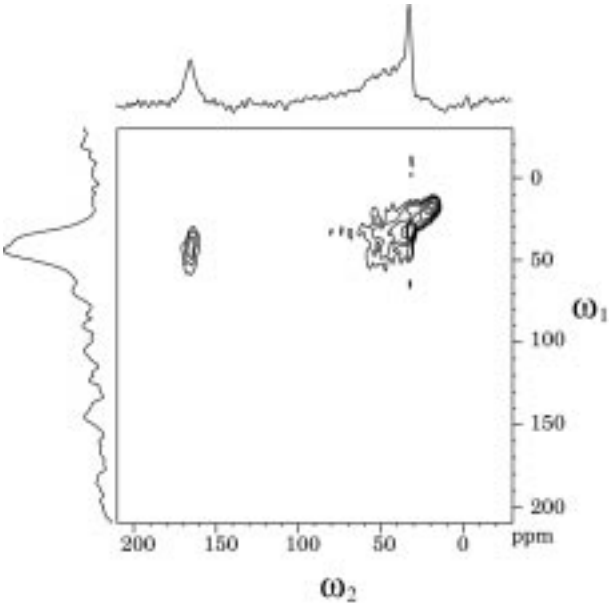

Figure 1. ^{13}C two-dimensional spectrum of $^{13}C_{1,\alpha}$-Gly_2 labeled gramicidin A in hydrated unoriented lipid bilayers. The projections of the cross peak region in the ω1 and ω2 dimensions are shown at the left and on the top of the contour plot. The spectrum was recorded on a Bruker DMX300 wide bore spectrometer system. 512 points were taken in the t_2 domain, and 320 scans were coadded for each of 64 t_1 experiments with a 22 μs dwell in both dimensions.

In Figure 1, a ^{13}C two-dimensional spectrum of an unoriented sample of $^{13}C_{1,\alpha}$-Gly_2 labeled gramicidin in hydrated lipid bilayers is presented. The $^{13}C_\alpha$ site has been selectively polarized by using a short (15 μs) contact time for cross polarization. In this way, the non-protonated carbons, such as $^{13}C_1$ do not have a chance to be cross polarized from the more distant, non-covalently attached protons. Following the selective polarization of the C_α site, and a variable interval for modulation of the signal for the two-dimensional experiment, a mixing time of 60 ms is used to transfer magnetization from C_α to C_1. The asymmetric 2D spectrum arises since transfer from C_1 to C_α is inhibited, because C_1 is not initially polarized, and hence does not give rise to a signal on the diagonal.

This selective communication between neighboring carbons may lead to an approach for signal assignment in multidimensional triple resonance spectra where both ^{13}C and ^{15}N signals could be correlated. Moreover, the selective polarization has lead to a reduced number of signals in the spectra, and hence a reduction in signal congestion. This is often a significant problem in the vicinity of the diagonal. Therefore, this experiment has shown potential for selectivity, resolution, and sensitivity that will all be needed for achieving resonance assignments.

Cation Binding Induced Changes in N-15 Chemical Shift Anisotropy in a Polypeptide

Tian, F., NHMFL/FSU, Chemistry
Cross, T.A., NHMFL/FSU, Chemistry and Molecular Biophysics

Chemical shifts reflect the electronic environment of the nucleus in both the chemical shielding tensor elements and in their isotropic average. Through studies of a polypeptide that binds cations the sensitivity of the tensor elements to the electron withdrawing capacity of the cations is assessed.

Gramicidin A, a hydrophobic polypeptide of 15 amino acid residue, forms, as a dimer, a monovalent cation selective channel across lipid bilayers. To conduct cations, this channel must first attract cations to its pore; hence the polypeptide has cation binding capabilities. The cation binding sites are composed of amide carbonyl groups from the polypeptide backbone. While it would be ideal to study the oxygen sites directly, we have chosen to work with the nitrogen sites of the same amide groups, because of a variety of spectroscopic advantages. These studies are complicated by the presence of a dynamic lipid environment. To achieve the static tensor element magnitudes in the presence and absence of cations the samples must be frozen or dried. The later choice leads to heterogeneity in the samples and the former does also unless the samples are very rapidly frozen. This is because the lipid bilayers have a gel to liquid crystalline phase transition, and samples lowered through this transition will be distorted from their native state. Consequently, an approach for rapidly plunging the samples to cryogenic temperatures has been developed in the laboratory analogous to the techniques used in electron microscopy for freeze-fracture methods. The cryogen used is liquid propane, and thin sample preparations at room temperature on a conducting surface are plunged into the cryogen. Following numerous repetitions of this process a large enough sample is accumulated in a liquid nitrogen bath for the solid state NMR spectroscopy. Shown in the figure are changes in the chemical shift tensor induced by cation binding to the amide groups of the polypeptide backbone.

Obtaining specific data on tensor element magnitudes in the presence and absence of cations or other electronic perturbants bound to molecular systems has been very challenging. Because gramicidin undergoes very little structural or dynamic change upon cation binding, the chemical shift data directly reports on the influence of electron withdrawal. It can also be shown that this is a through-bond effect, rather than a through-space polarization, because other amide groups that are not involved in cation solvation are unaffected (i.e. the tensors do not change) even though the nitrogen atoms for some of these sites are even closer to the cation.

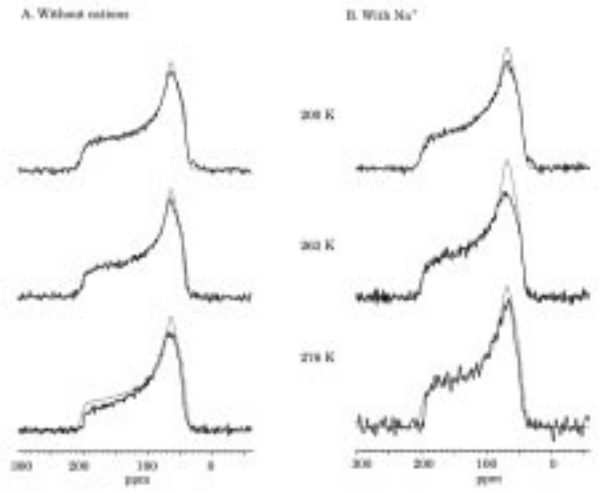

Figure 1. 40 MHz (9.4 T) ^{15}N chemical shift powder pattern spectra of fast frozen $^{15}N_{\alpha}$-Trp_{13} gramicidin in lipid bilayers hydrated with water or NaCl solution. The thin lines correspond to the best-fit simulations of the static 200 K spectra. The tensor element magnitudes at 200 K without cations are 204 ppm, 65.5 ppm, and 42.5 ppm (σ_{33}, σ_{22}, and σ_{11}, respectively) relative to a saturated solution of $^{15}NH_4NO_3$, and with Na^+ they are 199 ppm, 67 ppm, and 43 ppm, respectively. Approximately equal averaging of the tensor occurs as a function of temperature with and without cations.